Chemical Engineering Journal 144 (2008) 489–501

Contents lists available at ScienceDirect

Chemical Engineering Journal

journal homepage: www.elsevier.com/locate/cej

Performance and SEM characterization of Rh impregnated microchannel reactors in the catalytic partial oxidation of methane and propane

Bjørn Christian Enger[a], John Walmsley[b], Erlend Bjørgum[b], Rune Lødeng[b], Peter Pfeifer[c], Klaus Schubert[c], Anders Holmen[a], Hilde J. Venvik[a,*]

[a] Department of Chemical Engineering, Norwegian University of Science and Technology (NTNU), N-7491 Trondheim, Norway
[b] SINTEF Materials and Chemistry, N-7465 Trondheim, Norway
[c] Forschungszentrum Karlsruhe GmbH, Institute for Micro Process Engineering, Postfach 3640, DE-76021 Karlsruhe, Germany

ARTICLE INFO

Article history:
Received 10 March 2008
Received in revised form 27 June 2008
Accepted 14 July 2008

Keywords:
Synthesis gas
Hydrogen production
Microchannel reactor
Microstructured
Partial oxidation
Rhodium
Fecralloy
Nicrofer
Methane
Propane

ABSTRACT

Two different reactor materials (Fecralloy, Nicrofer) have been investigated in the catalytic partial oxidation of methane and propane. The focus of the study was on the stability and applicability of the different reactor materials, in particular their alumina coating related to their catalytic performance. Both reactors were impregnated using a $RhCl_3$ solution, yielding 6.3 and 4.6 mg of Rh deposited on the Fecralloy and Nicrofer, respectively.

It is shown that high temperature calcination of Fecralloy established a stable alumina coating. This effectively increased the surface area of the reactor providing sites for the Rh particles. The reactor performance was stable with both methane and propane feeds. SEM images of the Fecralloy reactor revealed significantly larger Rh particles near the reactor exit as compared to inside the reactor.

The Nicrofer was wash-coated with alumina using a sol–gel technique. SEM images of the Nicrofer reactor revealed the formation of Cr-layers and Cr-oxide structures covering the impregnated Rh particles. The Cr rich structures coating the Rh particles were found to be detrimental to the reactor performance, and the alumina wash-coating was consequently not successful at stabilizing the Nicrofer reactor material.

Methane was found to be more difficult to activate than propane, as expected, but provided the benefit of no formation of C_{2+} components, with H_2 and CO selectivities almost as high as with propane.

1. Introduction

The formation of synthesis gas by catalytic partial oxidation (CPO) of hydrocarbons is a well known process and has been reviewed regularly [1–7]. It is an emerging technology still not in commercial use, but it may have large benefits if it can be applied at conditions relevant to downstream applications. As an example, the theoretical H_2/CO ratio of the CPO process is optimal for gas-to-liquid (GTL) applications such as the Fischer–Tropsch synthesis. Furthermore, partial oxidation may be particularly interesting in fast start-up or dynamic response applications requiring a synthesis gas product, and the possibility of autothermal operation [8,9] is a desirable feature.

The conventional method for producing hydrogen is steam reforming (SMR), a process characterized by large multi-tubular reactors with external burners, and correspondingly large investment costs. It is therefore a goal to search for simpler, more compact, and less expensive methods. Small-scale distributed hydrogen production may be a target market area of the CPO process, although this requires a shift reactor to remove CO and increase the hydrogen yield. The products from methane partial oxidation combined with water-gas-shift (WGS) may consequently yield a gas composition favourable for CO_2 capture and sequestration.

CPO and microstructured reactors are examples of compact technologies, and may be considered in on-board applications for transportation purposes. Microstructured reactors are a relatively new invention that has received much attention in the last decade. Gas phase applications were recently reviewed by Kolb and Hessel [10]. Relevant to the present study are several reports, concerning both the production of hydrogen and synthesis gas, including studies of steam reforming [11–14], catalytic partial oxidation [9,15] and oxidative steam reforming (OSR) [15,16]. A heterogeneous reactor model for steam reforming of methane in a microchannel reactor has also been published [17].

Rh is one of the most extensively studied catalytic materials in the partial oxidation of hydrocarbons, and recent reports include [18–33]. It is also known to be among the elements with most promising properties for both steam methane reforming

* Corresponding author. Tel.: +47 735 92831; fax: +47 735 94080.
E-mail address: hilde.venvik@chemeng.ntnu.no (H.J. Venvik).

1385-8947/$ – see front matter © 2008 Elsevier B.V. All rights reserved.
doi:10.1016/j.cej.2008.07.055

[12,34–36] and dry reforming [37–41], and hence also autothermal reforming [42–44]. Some reports suggests that the dominant reaction pathway over Rh is the formation of CO [45], while CPO on most other metals appear to proceed through the formation of CO_2 and water, followed by subsequent reforming to synthesis gas [2–4,7,46]. This is, however, a controversial issue, and earlier results [47,48] including temporal-analysis-of-products (TAP) [49] indicated a combustion-reforming mechanism over Rh. This is supported by recent results using X-ray absorption spectroscopy (XAS) illustrating a 2-zone behaviour of a Rh catalyst [29,33], and spatially resolved species profiles [30]. Even though direct formation of CO and H_2 occurs over Rh in addition to their formation by reforming and shift, the operating conditions could be a key parameter in explaining suggested differences in mechanisms. Effects of contact time [18], gas phase contributions and surface species concentrations can be expected. Even if direct formation of H_2 and CO could be obtained at controlled and close to ultra-high-vacuum (UVH) conditions, this may not be the case when considering application relevant scale and conditions.

The purpose of the present work was to investigate two different reactor materials (Fecralloy, Nicrofer) in the catalytic partial oxidation of CH_4 and C_3H_8. The conditions were chosen based on our previous work [15,23,50]. In this study focus was put on the stability and applicability of Nicrofer as compared to Fecralloy, for which the stability has previously been reported based on more than 70 experiments of propane partial oxidation and oxidative steam reforming with no apparent deactivation [23]. In particular the different methods used for creating an alumina coating was of interest and the effect of this on catalytic performance. The reactor entrances, exits and channels were characterized using SEM.

2. Experimental

2.1. Reactor properties and impregnation

The metallic microchannel reactors (Fecralloy, Nicrofer) were manufactured at the Institute for Micro Process Engineering (IMVT) at Forschungszentrum Karlsruhe GmbH. The Fecralloy consisted of 72.6% Fe, 22% Cr and 4.8% Al [51]. The Nicrofer was a standard high temperature resistant alloy (3320H, typical application temperatures are 873–1123 K) consisting mainly of 30–32% Ni, 19–22% Cr and 46–51% Fe, but where small amounts of Mn, Si, Cu, Al and Ti are present. Physical characteristics for both reactors are shown in Table 1. The Fecralloy was a standard monolith while the Nicrofer contained a larger channel (600 μm × 600 μm) along the central axis to allow for temperature measurements inside the reactor, as was previously applied to a Fecralloy reactor in the same set-up [23,50].

The Fecralloy was oxidized at 1273 K for 4 h in order to form a thin alumina surface layer for supporting the catalyst and protecting the metallic microchannel reactor. This process has previously [50] been shown to increase the total surface area of the reactor by a factor of approximately 10 when compared to the geometric surface area of the channels. This ratio was based on earlier measurements using Kr-BET on an identical reactor where the total BET surface area was found to be 0.68 m^2 [15].

Table 1
Physical data for metallic microchannel reactors

Description	Fecralloy	Nicrofer
$H \times W \times L$ (mm^3)	5.5 × 5.6 × 20	5.5 × 5.6 × 20
No. of channels	676	572
Channel dimension (μm^2)	100 × 120	100 × 120
Geometric surface (cm^2)	59.5	50.3
Thermocouple channel (μm^2)	–	600 × 600
Void volume (cm^3)	0.162	0.144
Rh loading (mg)	6.3	4.6
Estimated heated dead volume in front (cm^3)	4.3	4.3

The Nicrofer was first annealed at 1073 K for 2 h with a heating rate of 3 K/min. The reactor was subsequently wash-coated with an alumina sol consisting of the following ingredients: 12.3 g Al-Sec-Butylat, 5 g Acetylacetonate, 8 g water, 50 g Isopropyl alcohol and HNO_3 (conc.) for a pH value of 4.5. The wash-coated reactor was dried at 343 K overnight and calcined at 1073 K for 4 h with a heating rate of 2.6 K/min. The total BET surface area by nitrogen sorption was 1.06 m^2.

Both reactors were impregnated using a Rh-chloride solution consisting of 250 mg $RhCl_3$ in 25 ml water. After impregnation the reactors were dried at 363 K for 4 h. Using the same Rh-chloride solution both reactors were impregnated 5–6 times, and the amount of Rh deposited was measured by mass increase to 6.3 mg on the Fecralloy and 4.6 mg on the Nicrofer. The reason for impregnating with relatively large amounts of Rh, compared to the 1 mg used previously [23,50], was the objective of studying the Rh crystallites inside the reactor channels using SEM. It was presumed that larger and a higher number of detectable crystallites would be obtained at higher loading.

The residence time τ inside each microchannel reactor was calculated at STP using Eq. (1), where $V_{channels}$ is the total volume of the channels and $Q_{tot,in}$ is the total volumetric gas flow into the channels.

$$\tau = \frac{V_{channels}}{Q_{tot,in}} \quad (1)$$

Selectivity to hydrogen was calculated based on the conversion of carbon feed, and selectivities to CO, CO_2 and C_{2+} were calculated based on a total carbon balance. Carbon mass balance closure was typically within ±1% and the retained ratio of H and O typically ranged from 1.9 to 2.1, indicating good closure on H and O balances by the formation of water, which was removed prior to GC analysis of the product stream.

2.2. Catalytic partial oxidation

Catalytic partial oxidation was carried out in co-feed modus, with the microstructured reactor fixed inside a tubular (12 mm) quartz housing, at near-to atmospheric pressure. The cylindrical reactor contained two quartz tubes (4 mm o.d.) with movable thermocouples for the measurements of gas temperatures, see Fig. 1. The reactor set-up and equipment for GC analysis has been described in more detail elsewhere [15,23,50,52]. The furnace temperatures and gas flows were typically in the range 573–973 K, and 9–36 Nl CH_4/h or 6 Nl C_3H_8/h, respectively. The impregnated reactors were reduced at 10 K/min from ambient to 1073 K followed by 2 h at 1073 K, in 30 Nml H_2/min + 270 Nml N_2/min. Previous investigations reported no observable deactivation after repeated experiments of heating and cooling [23], and the reactors were therefore only pre-treated before the first CPO experiment.

2.3. Steam reforming

Steam reforming of CH_4 was carried out at 1073 K. The feed consisted of 100 Nml CH_4/min + 150 Nml N_2/min, and the steam/carbon ratio was 2.5. The effect of adding a small amount of oxygen to the feed, a process known as oxidative steam reforming, was tested on the Fecralloy reactor by replacing 55 Nml N_2/min with air, effectively changing the total O/C ratio from 2.5 to 2.7.

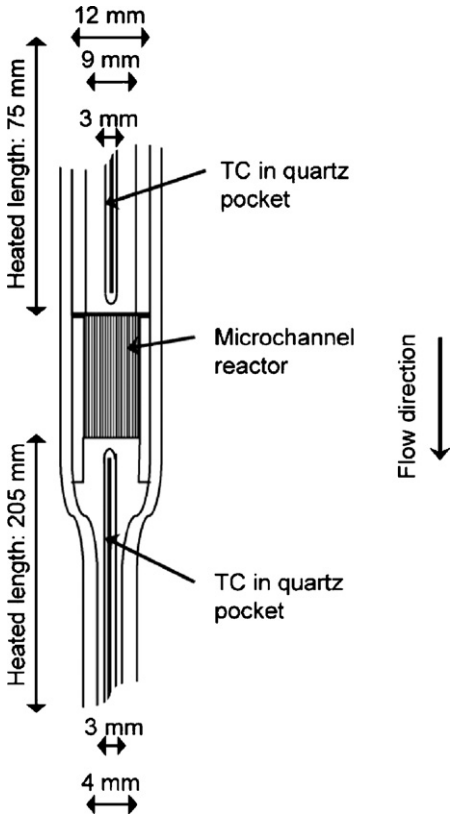

Fig. 1. Schematic drawing of the quartz reactor loaded with the metallic monolith [50].

2.4. SEM characterization

SEM was performed using a Hitachi S-4300SE instrument operated at beam voltages between 5 and 25 kV. Images were recorded using both secondary electron (SE) and backscattered electron (BSE) signals. Composition analysis of the surfaces was performed using an Oxford Instruments INCA system.

Reactor entrance and exit surfaces were examined in as-received condition after catalytic testing. They were then prepared in order to examine the inner channel surfaces. In order to prevent contamination or loss of material during cutting the channels were filled using a thermally setting mounting wax at about 373 K. After cooling, the reactors were cut transversely and longitudinally to provide internal sections parallel to the channel axes. The cut surfaces were polished using silicon carbide paper until a suitable row of channels were exposed. The thermal resin was then removed by standing the samples, polished face down, in acetone. After removal of the wax the sections were dried before SEM examination.

3. Results and discussion

3.1. Process conditions and reactor characteristics

The mass transport properties of the reactors were evaluated using the Reynolds and Peclét numbers, Eqs. (2) and (3) respectively, where d is the diameter of the channels inside the microreactors, ν is the linear flow velocity, ρ is the gas density, μ is the gas viscosity, z is a characteristic length scale and D is the diffusivity.

$$Re = \frac{\rho v d}{\mu} \tag{2}$$

$$Pe = \frac{vz}{D} \tag{3}$$

Based on the feed properties the Reynolds number inside the microchannel reactors was found to be less than 0.1, indicating a laminar flow regime. To check whether the Navier–Stokes equations can be applied, the Knudsen number was evaluated from Eq. (4), where k_B is Boltzmanns constant, T is the temperature, d is the molecular diameter, P is the pressure and L is the channel dimension.

$$Kn = \frac{k_B T}{\sqrt{2\pi} d^2 P L} \tag{4}$$

The Knudsen number is the ratio between the molecular mean free path and the channel dimension. When the Knudsen number is >0.1, Navier–Stokes cannot be applied as the number of wall collisions increase relative to intermolecular collisions. In this case the flow approaches molecular transport by Knudsen diffusion. When the Knudsen number is <0.001 Navier–Stokes describe the flow well. In our reactor, the Knudsen numbers of all relevant species were found to be in the range 0.001–0.1 in the temperature interval 473–1273 K. In this transition region between Navier–Stokes and molecular flow, the classical no-slip condition at the wall cannot be applied, and the flow inside the microchannels does not cause the formation of a viscous boundary layer near the channel wall. According to Kölbl et al. [53] the whole microchannel can be seen as a type of 'boundary layer' with fixed dimensions, where diffusion is the predominant radial mass transport mechanism.

The channel diameter in this study (100 μm × 120 μm) is smaller than the reported quenching distance of an explosive H_2/O_2 mixture (280 μm) at atmospheric pressure [54]. The safe conversion of a H_2/O_2 mixture has been reported by Janicke et al. [55] in a microchannel reactor with 140 μm × 200 μm channels, but more recent results have evidenced flame propagation through a heat exchanger operated without cooling (70 μm × 100 μm channels) at elevated pressures (20 bar) when igniting a H_2/O_2 mixture in a chamber upstream of the heat exchanger [56]. The inherent safety of using microchannel reactors may consequently depend on both the channel diameter, the pressure and strain due to temperature gradients.

The Peclét number was calculated using the reactor length (20 mm) as the characteristic length scale, which is sometimes referred to as the Bodenstein number (Bo). This is done in order to evaluate the ratio between mass transport by convection and diffusion. Based on a total flow of 1000 Nml/min it was found that the Bodenstein number was between 330 and 1000 (depending on the process conditions). The reactor length is 183 times the hydrolic diameter d_h of channels (109.1 μm), given by Eq. (5) where A is the cross sectional surface area of the channel and s is the length of the channel perimeter. As already mentioned, diffusion is the predominant radial mass transport mechanism, and considering the ratio between the Bodenstein number and L/d_h, the microchannel reactor operates as an axial PFR, but radially the gas mixing is closer to a CSTR.

$$d_h = \frac{4A}{s}, \qquad \frac{L}{d_h} = 183 \tag{5}$$

3.2. SEM characterization

Although the SEM characterization was carried out subsequent to the catalytic testing, the results are presented first because they have implications on the discussion and conclusions drawn from the experimental work.

Fig. 2 shows SEM images from the entrance of both the Fecralloy and Nicrofer reactor. By comparison the Nicrofer appears to be covered by a porous structure while the Fecralloy surface looks

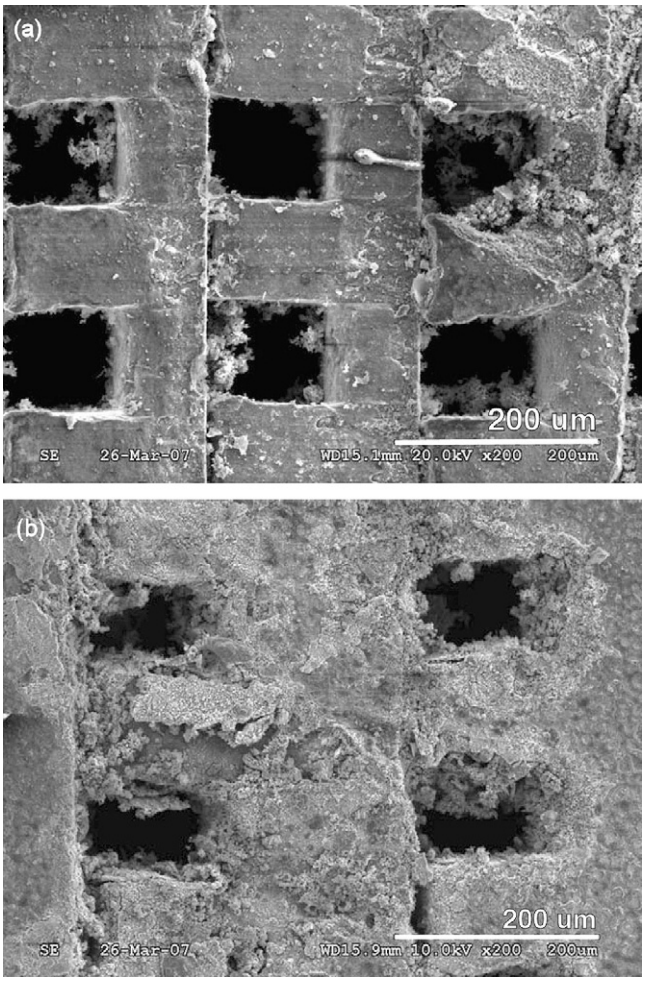

Fig. 2. Secondary electron (SE) SEM images obtained after catalytic testing showing reactor entrances. The channel dimensions are 100 μm × 120 μm. (a) Fecralloy reactor entrance obtained at 20 kV, 200× magnification, and (b) Nicrofer reactor entrance obtained at 10 kV, 200× magnification.

more dense. Fig. 3b illustrates Rh-particles (white) sitting in the porous structure at the Nicrofer reactor entrance, while on the Fecralloy large Rh clusters (white) can be seen covering the surface in Fig. 3a, in this case near the reactor exit. The large size of the imaged clusters near the reactor exit on the Fecralloy reactor may result from sintering during steam reforming at 1073 K after the catalytic partial oxidation. However, the impregnation method by which the Rh-chloride solution was introduced at the reactor entrance was observed to cause droplet formation at the reactor exit due to strong capillary forces. It is likely that this droplet formation affected the cluster size distribution inside the microchannels, effectively causing a larger deposition of rhodium near the reactor exit. Unfortunately, images were not taken before catalytic testing, or between CPO and SMR, which could have clarified this issue. FE-SEM images of a 0.01 wt% Rh/Al_2O_3 foam catalysts have previously shown that Rh particle sizes and distribution are modified in under partial oxidation and oxidative steam reforming conditions, and high concentrations of steam was observed to have a stronger impact on the stability of Rh than high temperatures in themselves [57].

By EDX analysis the amorphous structure on the Nicrofer was found to consist mostly of Cr-, Fe- and Al-oxides, although the presence of partially reduced Cr- or Fe-species cannot be excluded at conditions relevant to catalytic testing. H_2-TPR has shown that supported Fe_3O_4 is completely reducible [58], while supported CrO is only partially reducible [59]. Close examination of Fig. 3b reveals that Cr-oxide is covering or even enveloping the Rh particles (white). In contrast, the surface of the Fecralloy was found to be extremely rich in Al-oxide, with a much weaker signal from the Cr and Fe present in the reactor material. These results confirm that the high temperature calcination of the Fecralloy yielded a more dense alumina coating of the reactor material, whereas wash-coating the Nicrofer by using a sol–gel method did not prevent migration of Cr from the steel. The surface structures of Cr-oxide were most likely formed by segregation caused by destabilization of the reactor material at high temperatures in the reaction atmosphere. In a recent study by Stefanescu et al. [60] alumina wash-coating of Aluchrom microchannel platelets appears to have been sufficiently stable, at least for steam reforming applications. The stability of wash-coated metal surfaces in a strongly oxidizing atmosphere at high temperatures appears, however, to require more research to determine its possibilities and limitations.

Fig. 4 displays the microchannels inside the reactors after cutting. On the walls of the reactor channel, Rh particles of varying sizes are found. EDX analysis of the particles inside the Nicrofer reactor revealed the presence of bimetallic Rh-Ni species and even single Ni particles. Fig. 5a and b illustrates two sets of EDX data from inside the Fecralloy and Nicrofer reactor channels. As seen from Fig. 5b, Cr-

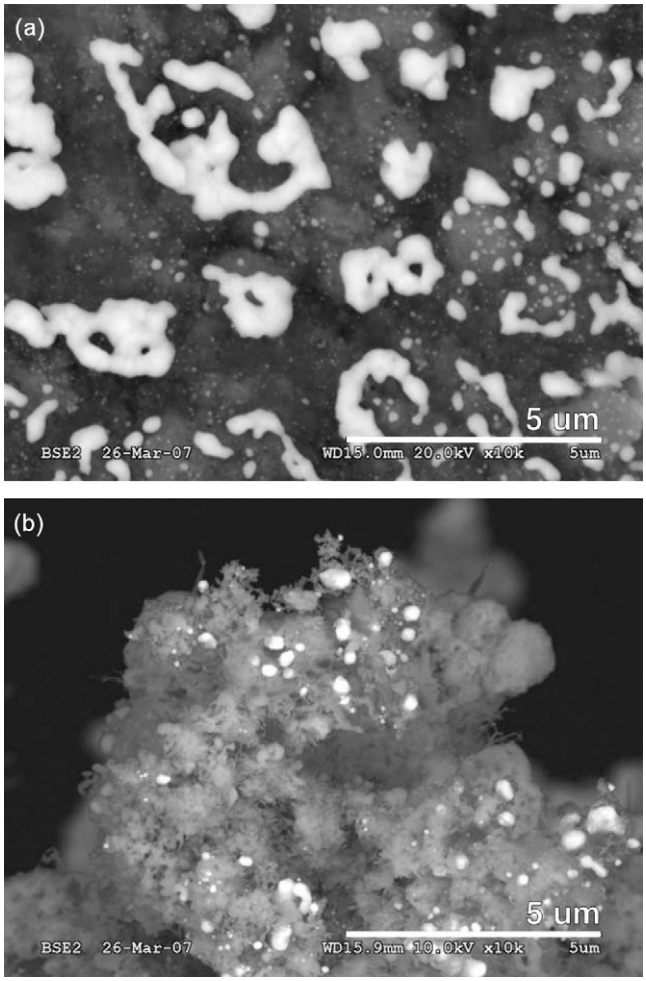

Fig. 3. Backscattering electron (BSE) SEM images of Rh-particles/clusters (shown in white) obtained after catalytic testing. (a) Rh clusters at the Fecralloy reactor exit obtained at 20 kV, 10^4× magnification, and (b) Rh particles at the Nicrofer reactor entrance obtained at 10 kV, 10^4× magnification.

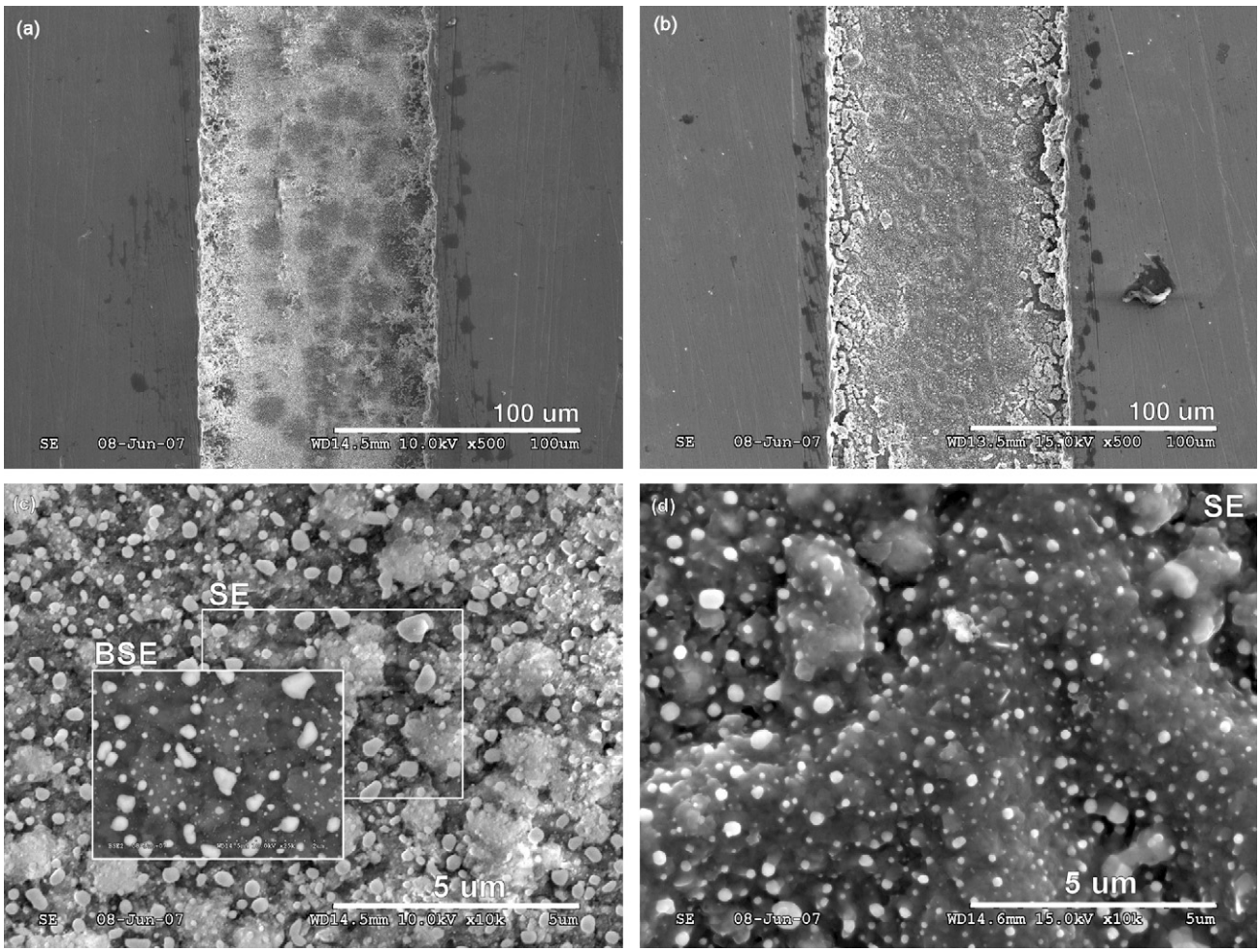

Fig. 4. Secondary electron (SE) SEM images of reactor channels obtained after catalytic testing and after cutting. Rh, Rh-Ni and Ni particles were located using BSE images and the Oxford Instruments INCA analysis system. (a) Fecralloy reactor channel obtained at 10 kV, 500× magnification, (b) Nicrofer reactor channel obtained at 15 kV, 500× magnification, (c) details inside the Fecralloy reactor channel obtained at 10 kV, $2.5 \times 10^4\times$ magnification, and (d) details inside the Nicrofer reactor channel obtained at 5 kV, $2.5 \times 10^4\times$ magnification.

and Fe-oxides were also present inside the Nicrofer reactor channels. The effect of a possible Rh-Ni alloy formation on the catalytic activity of the Rh particles in the Nicrofer reactor is uncertain. Basile et al. [61] reported no large overall effects of Rh-Ni synergy on the CPO of methane, except for Rh promoting the reduction of Ni and a slightly lower and broader temperature profile on the surface with increasing levels of Ni. Bimetallic formation on Rh-Ni catalysts has also been reported from experiments of dry reforming without any large negative effects [62–64]. The chemisorption of hydrogen has, however, been reported to diminish by the formation of bimetallic Rh-Ni particles [62].

3.3. Catalytic testing

Microstructured metallic reactors are especially well designed to study reactions at short/controlled residence times. High thermal conductivity provides an environment suited to dissipate the heat of reaction, which is a desirable property when performing experiments at controlled surface temperatures. Structured catalysts such as foams and monoliths [52,65] or powdered catalysts [43] have been shown to contain extreme hot-spots. Aartun et al. [23] reported temperature profiles obtained inside metallic microchannel reactors. However, steel has been found somewhat active for catalytic partial oxidation of methane [66], and since steel thermocouple pockets were necessary for the previously obtained temperature profiles, quartz pockets were used throughout the experiments in this study, which limited temperature measurements to the front and exit of the reactor. Examples of temperature profiles obtained during CPO with different feeds (propane and methane) are shown in Fig. 6.

3.3.1. CPO of propane

Fig. 7 shows that at steady-state conditions with a furnace temperature of 973 K the results obtained in the Fecralloy reactor were slightly better than in our previous study [50]. However, Aartun et al. [50] reported large effects of the residence time on conversion and selectivities, and the lower residence time in the study presented here could contribute to explain the increased selectivity of H_2 and CO. It is, however, more likely that the Rh-loading was the main contributor to the increased conversion and selectivities presented here. In fact, Aartun et al. [50] reported reduced conversion at residence times below 10 ms, but in our study we obtained higher conversion at 9.9 ms than at 12.7 ms in the former study. In either case, O_2-conversion was not complete at 973 K, which could have had a negative effect on the selectivity to partial oxidation products. To clarify the issue of residence times, the effect of changing the total flow, and thereby the linear velocity and residence time, was investigated by Aartun et al. [50]. However, the effect of using

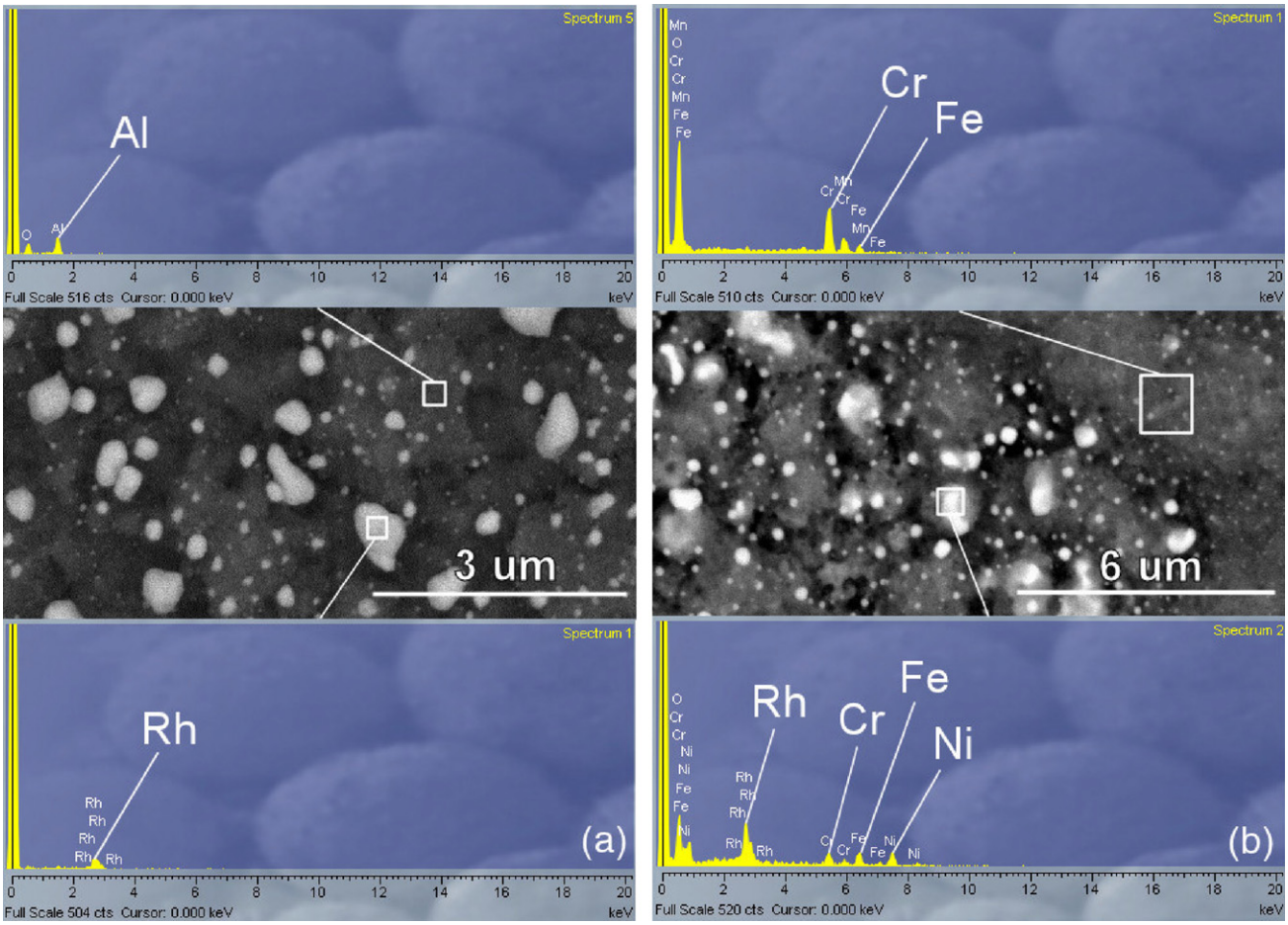

Fig. 5. Secondary electron (SE) SEM images of reactor channels obtained after catalytic testing and after cutting. Rh, Rh-Ni and Ni particles were located using BSE images and the Oxford Instruments INCA analysis system. (a) Fecralloy reactor channel obtained at 10 kV, 500× magnification; (b) Nicrofer reactor channel obtained at 15 kV, 500× magnification.

a longer reactor to change the overall residence time remains to be studied.

Analyzing the results from catalytic partial oxidation of propane at C/O = 0.8 reveals that there are large differences in reactor performance in terms of conversion and selectivity during heating (2 K/min) and cooling (1 K/min). Propane is activated at furnace temperatures above 750 K during heating, but conversion continues even at furnace temperatures below 550 K during cooling, as shown in Fig. 8a. However, the gas temperature near the reactor exit was measured to 800 K just before extinction. The H_2 selectivity during heating was strongly affected by the formation of dehydrogenation products and water. As shown in Fig. 8b it is particularly low in the

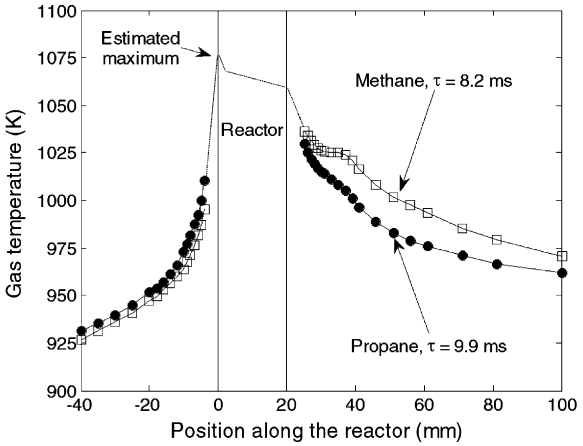

Fig. 6. Temperature profiles obtained during CPO of methane or propane over 6.3 mg Rh/Al_2O_3/Fecralloy at C/O = 0.8, and with 8.2 or 9.9 ms residence time for methane and propane, respectively. The maximum reactor temperature is estimated to about 1073 K based on a previous study [23].

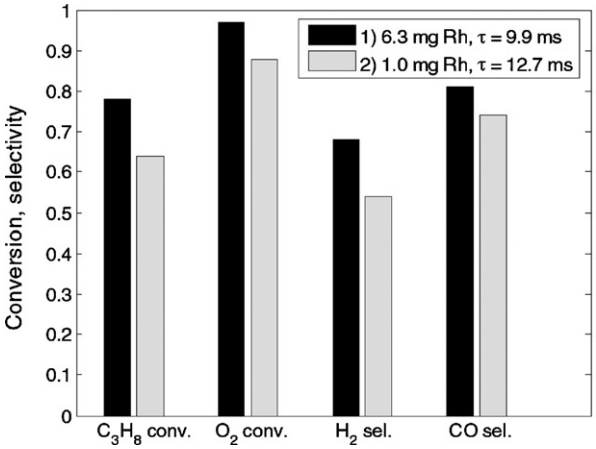

Fig. 7. Catalytic partial oxidation of propane over Rh/Al_2O_3/Fecralloy at C/O = 0.8 and a furnace temperature of 973 K. The results at steady-state (1) are compared with (2) the previous study of Aartun et al. [50].

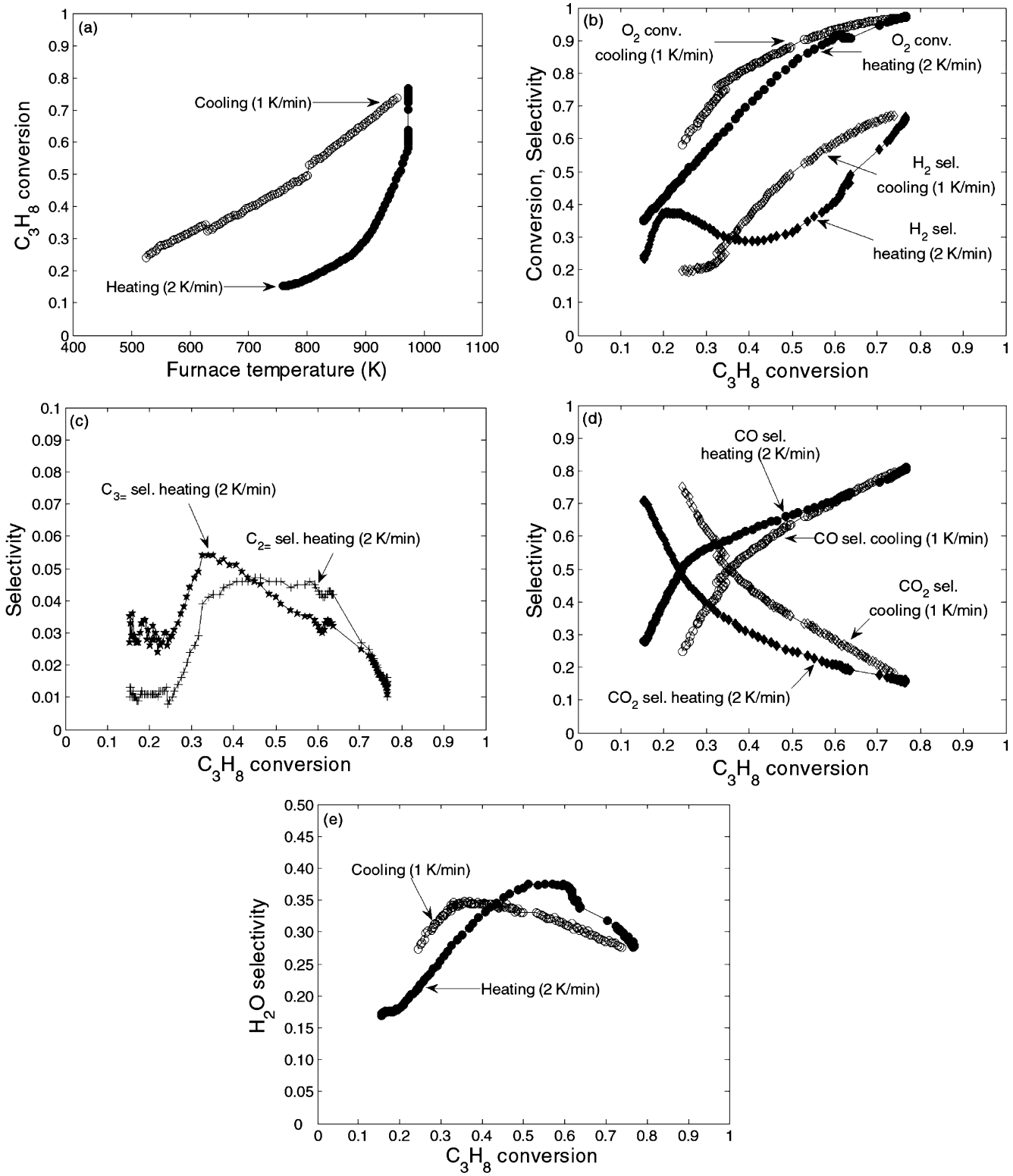

Fig. 8. Catalytic partial oxidation of propane over 6.3 mg Rh/Al_2O_3/Fecralloy at C/O = 0.8 and 9.9 ms residence time. The furnace temperature was increased at 2 K/min to 973 K, followed by 15–20 h steady-state operation, and then decreased at 1 K/min to ambient temperature. (a) Propane conversion as a function of temperature, and as a function of propane conversion: (b) O_2 conversion and H_2 selectivity, (c) the selectivity to $C_{2=}$ and $C_{3=}$, (d) the selectivity to CO and CO_2, and (e) the selectivity to H_2O.

propane conversion range 0.3–0.7, which is where the selectivity to dehydrogenation products, as depicted in Fig. 8d, is the highest. During light-off the CO selectivity plotted as a function of the propane conversion changes significantly at 25–30% propane conversion. This is seen in Fig. 8c, and the same is to some degree true for the selectivity to CO_2. The transition between these two regimes is less pronounced during cooling.

During cooling (1 K/min) the selectivity to $C_{2=}$ and $C_{3=}$ was < 0.01 at all times, and the selectivity to C_{2-} was always <0.003. Fig. 8d illustrates that during light-off there is a sudden increase in selec-

Table 2
Catalytic partial oxidation of methane at 973 K and 1 atm, after about 15 h

Reactor	τ (ms)	C/O	CH_4 conv. (%)	O_2 conv. (%)	H_2 sel. (%)	CO sel. (%)
Fecralloy	8.2	0.8	58	95	59	73
Fecralloy	19.2	1.0	53	99	67	79
Fecralloy	9.6	1.0	54	97	69	80
Fecralloy	4.8	1.0	57	96	74	84
Nicrofer	7.3	0.8	10	25	20	34
Nicrofer	17.1	1.0	15	55	15	34
Nicrofer	8.5	1.0	11	35	25	41

tivity to partially dehydrogenated products. The H_2O selectivity also peaked in the same conversion range, as shown in Fig. 8e. Because the selectivity to ethane was low (<0.3% C-basis) both during heating and cooling, the rate of recombination chemistry, i.e. $CH_3 + CH_3 \rightarrow C_2H_6$ or $C_2H_5 + H \rightarrow C_2H_6$ appears to be very low. If recombination chemistry on the catalyst surface was the source of ethene, then higher levels of ethane might be expected since the CH_3 and CH_2 surface species have almost the same dehydrogenation barrier (at STP) on Rh(1 1 1) [67]. It could, however, be that Rh(1 1 1) is not representative for the working catalyst.

The results from catalytic partial oxidation of propane in the Nicrofer reactor are given in Fig. 9. Conversion and selectivities were highly unstable during operation at steady-state conditions and 973 K furnace temperature. After run (1) the reactor was therefore oxidized at 1123 K for 2 h to see if this could stabilize its performance and then tested once in the catalytic partial oxidation of methane before subsequent runs with propane were carried out. The oxidation appears to have stabilized the selectivity to CO (Fig. 9b), but the reactor conversion of propane and oxygen were decreasing with time on stream (Fig. 9a). The larger decrease in oxygen conversion, as compared to propane conversion, is caused by the increased selectivity to dehydrogenation products, as seen in Fig. 9c. The deactivation process affecting the conversion appeared to be permanent. The results in the Nicrofer reactor cannot be compared directly to the Fecralloy reactor. The uncertainty in flow distribution and residence time introduced by the axial thermocouple channel in the Nicrofer reactor is the main reason for this. The very low selectivity to hydrogen in the Nicrofer reactor during steady-state operation, as compared to the Fecralloy reactor, can be explained by the much higher selectivity to ethene and propene (Fig. 9c vs. Fig. 8c), and about 10% higher selectivity to water (Fig. 9b vs. Fig. 8e).

Even though the Nicrofer contained 4.6 mg Rh, the SEM investigation after reaction experiments showed that a large portion of this Rh had been covered by Cr-oxide and was consequently not available to reactants. The high selectivity to dehydrogenated products could be related to the dehydrogenation activity of Cr [68], and the low availability of Rh. The combustion activity of Cr- and Mn-oxides [69] may also have been of some importance. In conclusion, if Nicrofer is to be used in catalytic partial oxidation of propane or a similar process, then it is essential that the surface coating is sufficiently dense and highly stable. Cr will otherwise segregate to the surface, and with time on stream migrate to cover the deposited catalyst, in this case Rh.

3.3.2. CPO of methane

The catalytic partial oxidation of methane was investigated in both reactors (Fecralloy, Nicrofer). Results at steady-state conditions, 973 K furnace temperature, are shown in Table 2. For the same reasons as discussed above, the performance of the Nicrofer reactor in terms of both conversion and selectivities was poor when methane was fed.

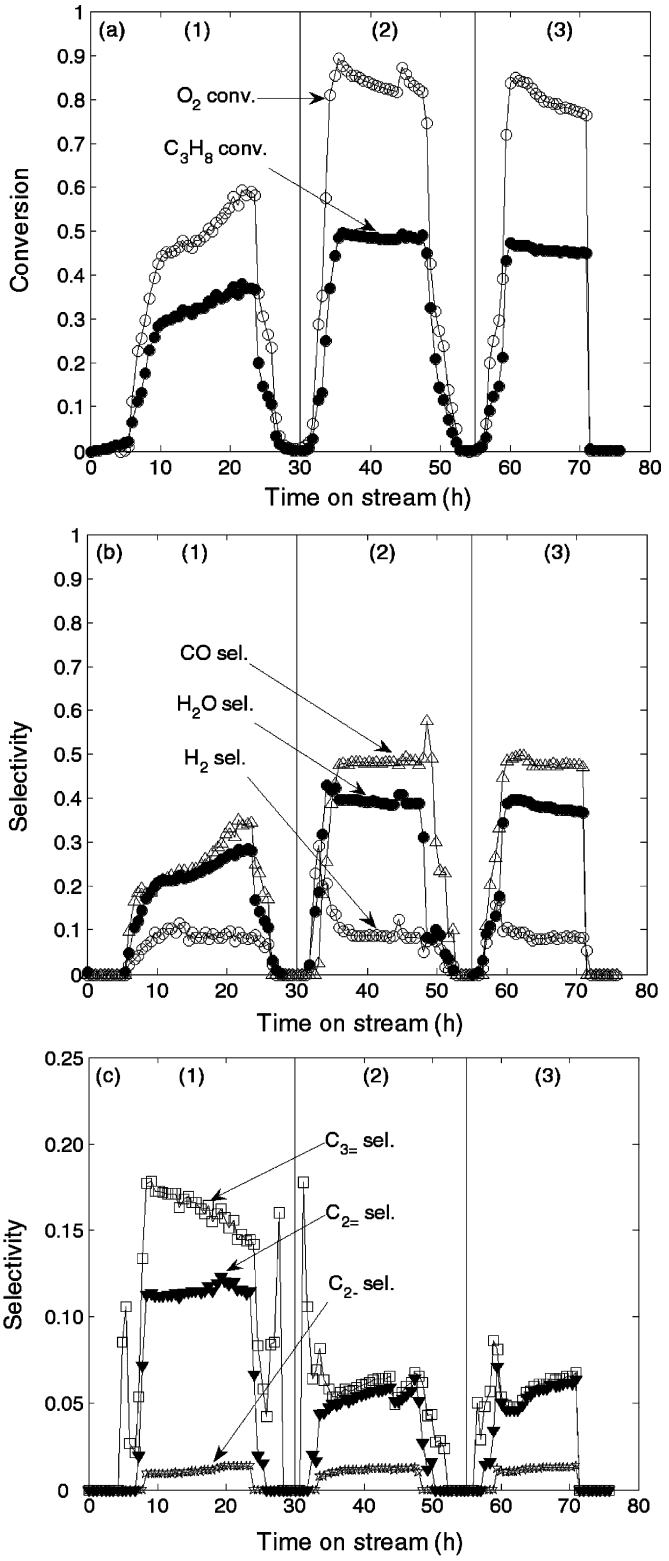

Fig. 9. Catalytic partial oxidation of propane over 4.6 mg Rh/Al_2O_3/Nicrofer at C/O = 0.8 and 8.8 ms residence time. The furnace temperature was increased at 2 K/min to 973 K, followed by 15–20 h steady-state operation, and then decreased at 1 K/min to ambient temperature. Run (1) was followed by oxidation at 1123 K for 2 h and one experiment with methane before runs (2) and (3) were carried out. As a function of time on stream showing (a) propane and oxygen conversion, (b) the selectivity to H_2 and CO and (c) the selectivity to dehydrogenated products (ethane, ethene and propene).

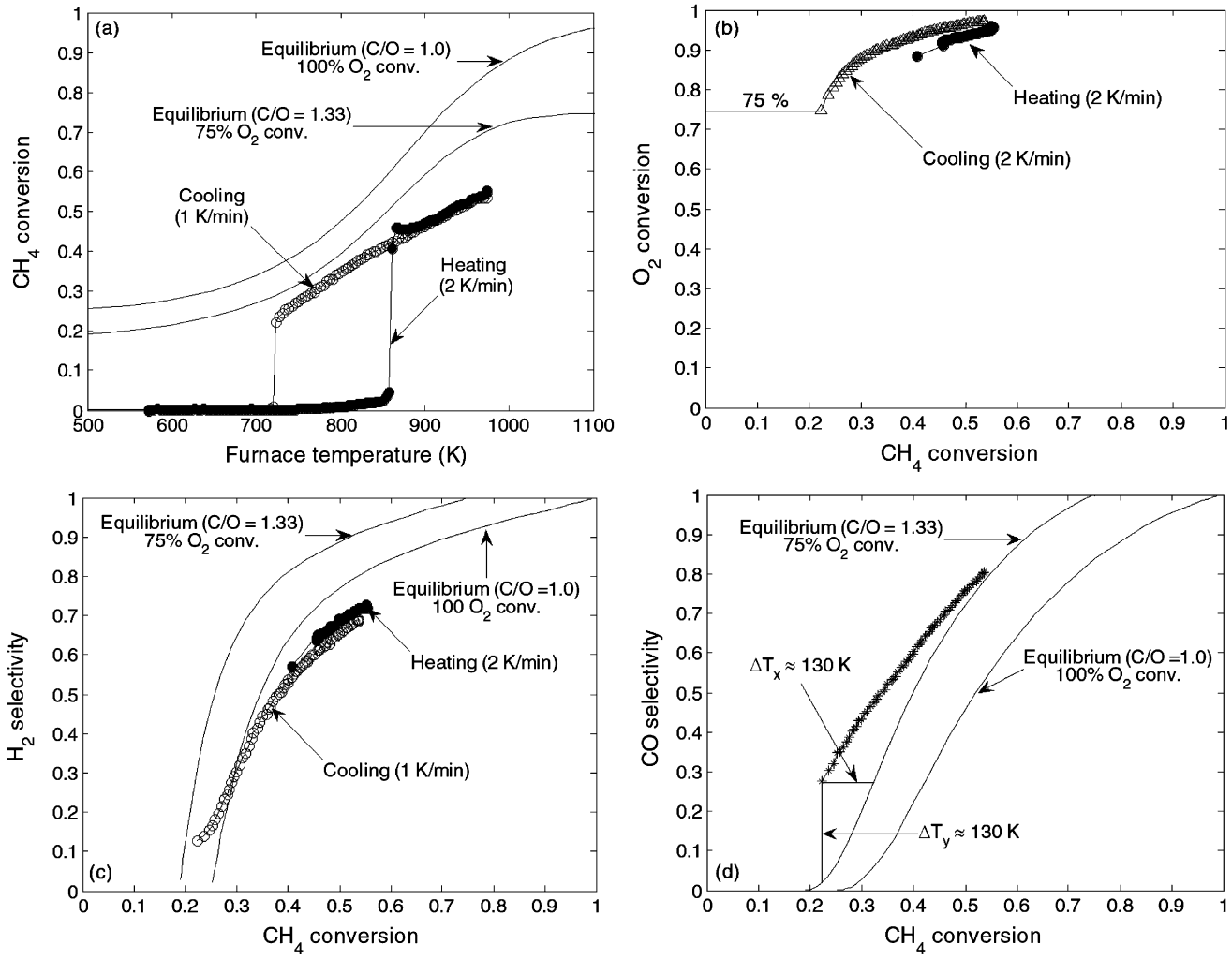

Fig. 10. Catalytic partial oxidation of methane over 6.3 mg Rh/Al_2O_3/Fecralloy at C/O = 1.0 and 9.6 ms residence time. The furnace temperature was increased at 2 K/min to 973 K, followed by 15–20 h steady-state operation, and then decreased at 1 K/min to ambient temperature. (a) The light-off plot for CH_4 as a function of temperature, and as a function of CH_4 conversion: (b) O_2 conversion, (c) H_2 selectivity and (d) the selectivity to CO.

Fig. 10a illustrates that the activation of methane in the Fecralloy reactor was almost instantaneous once the furnace reaches about 850 K. After light-off, increasing the temperature further caused an almost linear increase in the conversion of methane. The reaction carried on at lower furnace temperatures during cooling, and the gas temperature measured at the reactor exit was about 923 K (compared to a furnace temperature of about 723 K), just before extinction. This indicates that under the present conditions, activation of methane begins about 100 K higher than for propane. The fact that methane is more difficult to activate is expected from comparing the gas phase C–H bond dissociation energy of methane (439.3 kJ/mol) to the gas phase C–H (422.2 kJ/mol) or the C–C (370.3 kJ/mol) bond dissociation energies of propane [70].

The conversion of O_2 was always <100% (Fig. 10b). This was most likely not beneficial for the selectivity to partial oxidation products since the entire length of the reactor channels would be possible sites for oxidation chemistry subsequent to H_2 or CO formation. Fig. 10c and d compare the selectivity as a function of the methane conversion with the thermodynamic equilibrium values. Because the oxygen conversion was <100%, two equilibrium lines have been included corresponding to equilibrium at C/O = 1.0 (100% O_2 conversion) and at C/O = 1.33 (75% O_2 conversion). This is necessary because O_2 conversion is always complete in the thermodynamic calculations. In an exothermic process the furnace temperature represents a lower limit for comparing experimental data to the thermodynamic equilibrium. The maximum surface temperature provides an upper limit. The methane conversion and H_2 selectivity in this study never reached equilibrium vales, not even at the lower limit with 75% O_2 conversion, as illustrated in Fig. 10a and c.

Plotting the selectivity versus the conversion of methane, and then comparing with the equilibrium values, is a tool for evaluating whether there exists a direct route to the desired products (H_2 and CO) according to the ideal CPO reaction (6), or if global thermodynamics is controlling the product selectivity. Because the reaction of methane and oxygen is practically irreversible, Eq. (6) is written only in the forward direction to reflect this property of a direct route. The described analysis, however, requires the comparison of temperature differences that can be found by expressing the equilibrium conversion and selectivities as functions of the temperature. Fig. 10d illustrates this process where a point on the experimental CO curve is compared to the equilibrium curve at that specific conversion and CO selectivity. Because the oxygen conversion was <100%, only one point is here compared, in this case at 75% O_2 conversion. When compared to equilibrium, $\Delta S(\mathrm{CO})$ and $\Delta X(\mathrm{CH_4})$ correlate to the changes in temperature ΔT_y and ΔT_x, respectively. If there was a detectable direct route to CO according to reaction (6), then $\Delta T_y > \Delta T_x > 0$ must be required, while in our case

$\Delta T_x = \Delta T_y$.

$$CH_4 + 0.5O_2 \rightarrow CO + 2H_2 \quad (6)$$

As equilibrium conversion was never reached, Fig. 10d can therefore be interpreted to illustrate that reactions subsequent to methane activation are shifting the product selectivities closer to their equilibrium values, and that temperatures above bed exit gas temperatures are affecting the selectivities. Since the CO and CO_2 selectivities appears to be shifted proportionally, relative to equilibrium, the water-gas-shift reaction may be important. Calculating the Q value from the WGS equilibrium, Eq. (7), using experimental data at 1039 K bed exit gas temperature gives $\log(Q) = -0.25$, and the ratio between Q and the thermodynamic K at 1039 K is $Q/K = 10^{-0.25}/10^{0.09} = 0.457$, which indicates an approach to equilibrium at bed exit gas temperatures. Considering that the conditions inside the reactor are different from those in the ideal WGS reaction, there appears to be a significant effect of the WGS reaction. However, this does not exclude the possibility that direct formation of partially oxidized products may have occurred at some point inside the reactor, it is just not possible to claim a direct route when considering the available data and global thermodynamics.

$$Q = \frac{p_{CO_2} p_{H_2}}{p_{CO} p_{H_2O}} \quad (7)$$

Such a procedure of comparing experimental results to equilibrium calculation is unnecessarily elaborate if the true reaction temperature is known. In the catalytic partial oxidation, however, establishing the correct process temperature is typically not possible due to strong gradients. An option would be to compare with upper and lower limits on equilibrium values, as determined from the measured maximum and minimum temperatures in the reaction zone at a given furnace temperature. Again, in the catalytic partial oxidation of methane the upper limit or actual surface temperature is difficult to measure [43,71–73]. The mentioned approach circumvents this problem by relying only on the gas composition analysis. No temperature measurements have been used in the given evaluation.

3.3.3. SMR/OSR of methane

Both reactors were tested in the steam reforming of methane, but the Nicrofer reactor did not yield any conversion at 1073 K with S/C = 2.5. This result could indicate a very low surface area of Rh, that the Rh-Ni bimetallic or Ni particles were not sufficiently active or that the residence time was too short for CH_4 activation. The Fecralloy reactor, however, proved to be active at the same conditions, but the activity decreased with time on stream, from an initial 18.5% conversion to 11.5% after 3 h. The H_2 selectivity was constant at about 60% while the CO selectivity decreased from 60 to 52%. The process was subsequently switched to oxidative steam reforming, and the conversion increased to 14–15%. Adding oxygen to the feed was more detrimental to the H_2 selectivity (dropping to 35–38%) than to the CO selectivity (dropping to 50%). When switching back to steam reforming, the reactor had apparently deactivated further, and only 10% conversion was reached after 8 h on stream. The selectivites to H_2 and CO returned to the same levels as before OSR.

The most likely reason for the observed deactivation is migration and sintering of Rh-particles [57]. The size of the Rh-clusters found at the reactor exit in Fig. 3a, are substantially larger than those seen inside the reactor channel, Fig. 4c. However, it cannot be ruled out that the impregnation procedure was responsible for some of the observed differences since no SEM images were taken on freshly reduced reactors before they were exposed to reactants. SEM imaging from inside the channels would in any case not be possible until after the reactors had been destroyed by cutting.

3.3.4. Mechanisitic considerations regarding methane versus propane

Even though methane is more difficult to activate, the benefit of using methane instead of propane is that the selectivity to C_{2+} components was below detection limits (<0.0001) during CPO at a furnace temperature of 973 K (or lower) and 1 atm. For propane, the selectivity to C_{2+} components was found to increase with increasing furnace temperature, in accordance with previous results [23,50].

The catalytic conversion of propane with oxygen is a complex system where both heterogeneous and homogeneous processes may contribute [74], and the C_3H_8/O_2 ratio is a determining factor for the product selectivity [75,76]. At a residence time of 3 s inside a high purity alumina tube the oxidative dehydrogenation of propane reaches high conversion, even in the absence of a catalyst with only quartz filling in the reactor [77].

Fig. 11 illustrates some major routes in the conversion of propane, where thermal and catalytic cracking, dehydrogenation (DH) and oxidative dehydrogenation (ODH) are important reactions. These may occur either in the gas phase, on the catalyst, or on the support.

Our results showed high selectivity to ethene and propene in the Nicrofer reactor. In the presence of oxygen, an ODH route where hydrogen is removed from propane, either directly or after C–C scission, could help explain our results. The low selectivity to ethane could be a result of free oxygen atoms or O_2 scavenging hydrogens from C_2H_y fragments. It is likely that ODH reactions dominate near the reactor entrance and that DH reactions take over closer to the reactor exit where the concentration of free oxygen is expected to be lower. The ODH reactions are also a source of water through the inherent formation of OH groups, either directly on the surface or indirectly through the gas phase specie $HO_2^{\bullet}$ followed by H_2O_2 which decomposes to OH on the surface. This water may be converted to hydrogen through subsequent SMR or WGS, while the DH reactions provide an indigenous route to hydrogen.

The high selectivities to ethene and propene observed in the Nicrofer are in agreement with Huff and Schmidt [75], who studied oxidative dehydrogenation of propane on Pt and Rh impregnated monoliths at short contact times (5 ms). It was also shown that increasing the flow rate, and thereby reducing the residence time, caused an increase in the selectivity to propene, as well did increasing the amount of dilutant N_2 [75]. It is therefore possible that the high selectivities to dehydrogenated products in our study were affected by the lower residence time in the Nicrofer compared to the Fecralloy reactor. Since air was used in the experiments, the concentration of dilutant N_2 was high (above 70% of total feed).

Higher hydrocarbons (C_{4+}) is typically formed by free radical chain reactions in the gas phase [74]. In the Nicrofer reactor trace amounts of C_{4+} was detected. This is most likely an indication that gas phase chemistry infront of or inside the reactor has contributed to the conversion of propane. An insufficient catalytic surface to convert the C_{4+} components could help explain the results. Since the microchannels are much smaller than the quenching distance for an explosive C_3H_8/O_2 mixture (1.73 mm) [54], it is uncertain to which extent gas phase reactions inside the channels are contributing to the chemistry. However, from the mentioned calculation of the Knudsen numbers, being in the interval 0.001–0.1 in the temperature range 473–1273 K, collisions in the gas phase are more frequent than collisions with the catalytic surface.

Aartun et al. [15] tested a high temperature calcined Fecralloy reactor before Rh impregnation and found 30% propane conversion and 87% O_2 conversion at 1073 K product gas temperature and 9.7 ms residence time. No formation of H_2 was detected at this temperature, but 12% selectivity to CO was obtained. It is uncertain

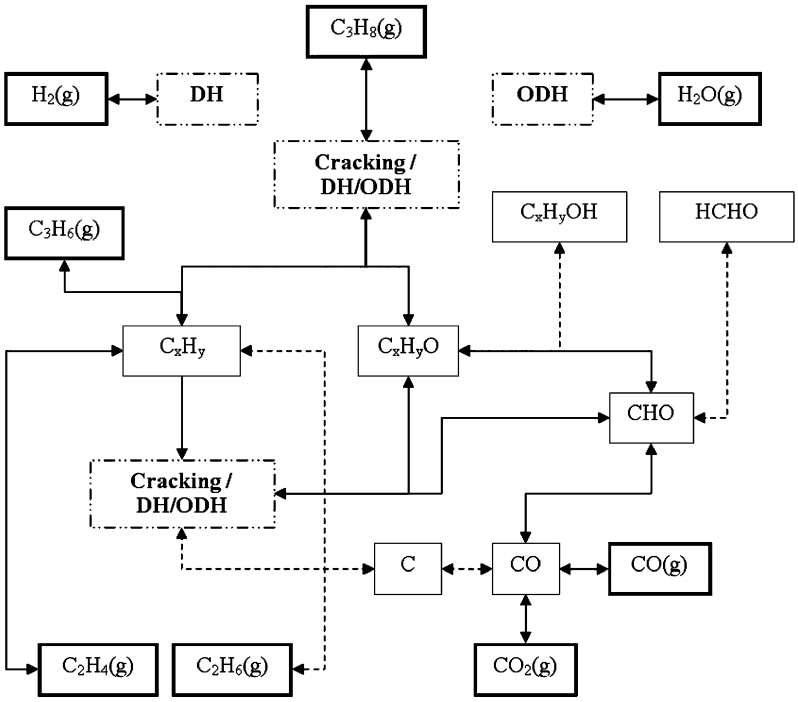

Fig. 11. Illustration of suggested important reaction pathways (solid lines) and less important pathways (dashed lines) in the CPO of propane, based on the obtained results (product selectivities).

whether this conversion was catalysed by the alumina wash-coat together with the Fecralloy itself, or if it was purely gas phase chemistry infront of or inside the microchannel reactor. Aartun et al. [23] reported significant ignition infront of the reactor at a reactor temperatures above 1023 K.

The oxidative pyrolysis of propane in the gas phase may proceed via a chain radical mechanism, and according to Beretta et al. [76] the ODH reaction, Eq. (8), requires only 192.5 kJ/mol as compared to 366.1 kJ/mol for the cracking, Eq. (9).

$$C_3H_8 + O_2 \rightarrow HO_2 + C_3H_7 \quad (8)$$

$$C_3H_8 \rightarrow CH_3 + C_2H_5 \quad (9)$$

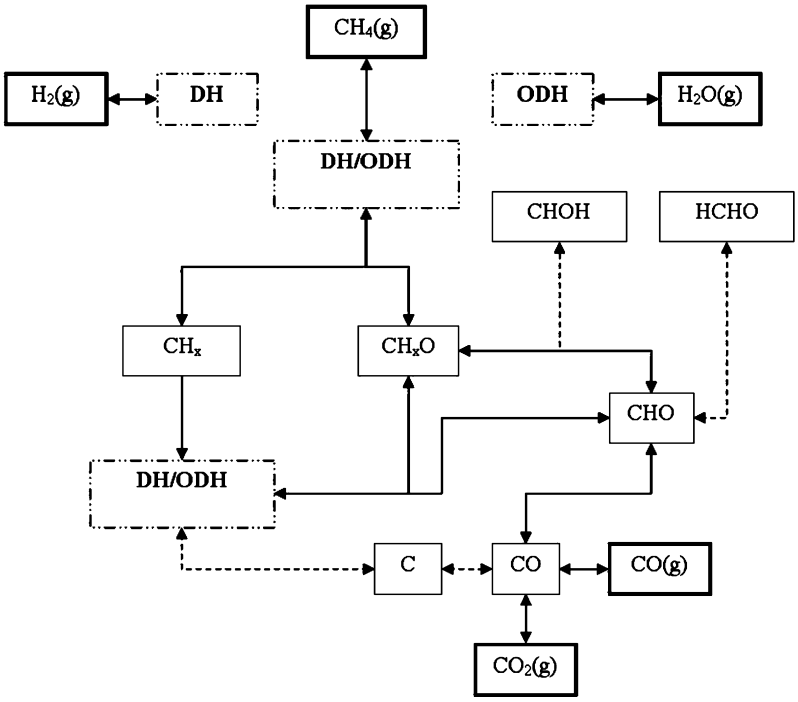

Fig. 12. Illustration of suggested important reaction pathways (solid lines) and less important pathways (dashed lines) in the CPO of methane, based on the obtained results (product selectivities).

Based on simulations, high conversion at only 3 ms contact time was predicted for the ODH process, while the pyrolysis process required 24 ms [76]. Comparing this to the conditions inside our microchannel reactors, there is more than enough time to activate propane and form dehydrogenated products through a gas phase ODH process.

The possibility of alcohol or aldehyde formation is also illustrated in Fig. 11. The condensate was not analyzed for alcohols or aldehydes. However, the carbon mass balances were good, and any significant formation of carbon rich condensates should have caused a deviation. If such products were formed to any significant extent inside the reactor, they were not stable under the present conditions.

Massive build-up of carbon deposits breaking off from the catalytic surface would have been detected through fouling of filters downstream of the reactor causing an increased pressure drop in the system. The pressure was not found to increase during testing with methane or propane, and high rates of carbon formation are consequently unlikely. Again the carbon mass balances would have shown significant deviations if high rates of carbon formation had occurred. Carbon deposition can be expected on Ni, but Rh is known to be resistant toward carbon formation[78,79].

Fig. 12 illustrates the catalytic conversion of methane with oxygen. Compared to the mechanism for propane in Fig. 11 it is simpler and the observed products did not include ethane, ethene or propene. The absence of thermal or catalytic cracking helps reduce gas phase contributions to the reaction mechanism, and evidently increases the carbon selectivity to CO/CO_2. According to Holmen et al. [80] gas phase decomposition of CH_4 at short residence times typically requires temperatures in excess 1400 K, as compared to the observed 1040 K bed exit gas temperature in this study. The low temperature and absence of C_{2+} from methane is thus an indication that gas phase reactions with CH_x are less likely as compared to propane, but gas phase contributions to the combustion, i.e. of H_2 cannot be ruled out.

4. Conclusions

It has been shown that high temperature calcination of Fecralloy yielded a stable alumina coating which is vital to the stability and performance of the reactor during catalytic partial oxidation of methane and propane. Wash-coating a Nicrofer reactor with alumina using a sol–gel technique failed to provide a similar surface coating and stability. Significant formation of Cr-layers and Cr-oxide structures, covering the Rh particles and channel surfaces, respectively, was detailed inside and outside the Nicrofer reactor using electron microscopy.

The Fecralloy reactor yielded results in accordance (or even better) than what has been published previously. The Nicrofer reactor, which could not be directly compared to the Fecralloy reactor due to a large axial channel, was found to yield high levels of the dehydrogenated products ethene and propene. The DH/ODH activity of the Cr metal or metal oxide layers coating the Rh particles may have contributed to this result, but gas phase radical reactions were most likely also present, as indicated by the presence of trace amounts of C_{4+} components in the product stream from the Nicrofer reactor.

Converting methane to synthesis gas inside the microchannel reactors was found to be slightly more difficult than the conversion of propane. This was most likely a direct cause of the difficulty in activating the C–H bonds of methane compared to the C–H and C–C bonds of propane. A benefit of using methane was no formation of C_{2+} components, and H_2 and CO selectivities almost as high as with propane.

Acknowledgments

The financial supports of the Research Council of Norway, and StatoilHydro through the RENERGI program, and the Norwegian University of Science and Technology (NTNU) are greatly acknowledged.

References

[1] S.S. Bharadwaj, L.D. Schmidt, Fuel Process. Technol. 42 (1995) 109.
[2] S.C. Tsang, J.B. Claridge, M.L.H. Green, Catal. Today 23 (1995) 3.
[3] S.C. Reyes, J.H. Sinfelt, J.S. Feeley, Ind. Eng. Chem. Res. 42 (2003) 1588.
[4] A.P.E. York, T. Xiao, M.L.H. Green, Top. Catal. 22 (2003) 345.
[5] Y.H. Hu, E. Ruckenstein, Adv. Catal. 48 (2004) 297.
[6] A.P.E. York, T.-C. Xiao, M.L.H. Green, Catal. Rev.-Sci. Eng. 49 (2007) 511.
[7] B.C. Enger, R. Lødeng, A. Holmen, Appl. Catal. A 346 (2008) 1.
[8] D.A. Hickman, L.D. Schmidt, Science 259 (1993) 343.
[9] M. Fichtner, J. Mayer, D. Wolf, K. Schubert, Ind. Eng. Chem. Res. 40 (2001) 3475.
[10] G. Kolb, V. Hessel, Chem. Eng. J. 98 (2004) 1.
[11] Y. Men, H. Gnaser, R. Zapf, V. Hessel, C. Ziegler, G. Kolb, Appl. Catal. A 277 (2004) 83.
[12] G. Kolb, R. Zapf, V. Hessel, H. Löwe, Appl. Catal. A 277 (2004) 155.
[13] A. Tonkovich, S. Perry, Y. Wang, D. Qui, T. LaPlante, W. Rogers, Chem. Eng. Sci. 59 (2004) 4819.
[14] C. Cremers, A. Pelz, U. Stimming, K. Haas-Santo, O. Görke, P. Pfeifer, K. Schubert, Fuel Cells 7 (2007) 91.
[15] I. Aartun, T. Gjervan, H. Venvik, O. Görke, P. Pfeifer, M. Fathi, A. Holmen, K. Schubert, Chem. Eng. J. 101 (2004) 93.
[16] C. Horny, L. Kiwi-Minsker, A. Renken, Chem. Eng. J. 101 (2004) 3.
[17] C. Cao, Y. Wang, R.T. Rozmiarek, Catal. Today 110 (2005) 92.
[18] A. Beretta, P. Forzatti, Chem. Eng. J. 99 (2004) 219.
[19] K.A. Williams, C.A. Leclerc, L.D. Schmidt, AIChE J. 51 (2005) 247.
[20] S. Rabe, T.-B. Troung, F. Vogel, Appl. Catal. A 292 (2005) 177.
[21] T. Bruno, A. Beretta, G. Groppi, M. Roderi, P. Forzatti, Catal. Today 99 (2005) 89.
[22] C. Cellier, D. Le Clef, C. Mateos-Pedrero, P. Ruiz, Catal. Today 106 (2005) 47.
[23] I. Aartun, H.J. Venvik, A. Holmen, P. Pfeifer, O. Görke, K. Schubert, Catal. Today 110 (2005) 98.
[24] A. Schneider, J. Mantzaras, P. Jansohn, Chem. Eng. Sci. 61 (2006) 4634.
[25] R. Wang, H. Xu, X. Liu, Q. Ge, W. Li, Appl. Catal. A 305 (2006) 204.
[26] W.-Z. Weng, X.-Q. Pei, J.-M. Li, C.-R. Luo, Y. Liu, H.-Q. Lin, C.-J. Huang, H.-L. Wan, Catal. Today 117 (2006) 53.
[27] P. Arpentinier, F. Basile, G. del Gallo, P. Fornasari, D. Gary, V. Rosetti, A. Vaccari, Catal. Today 117 (2006) 462.
[28] I. Tavazzi, A. Beretta, G. Groppi, P. Forzatti, J. Catal. 241 (2006) 1.
[29] J.-D. Grundwaldt, S. Hannemann, C.G. Schroer, A. Baiker, J. Phys. Chem. B 110 (2006) 8674.
[30] R. Horn, K.A. Williams, N.J. Degenstein, L.D. Schmidt, Chem. Eng. Sci. 62 (2007) 1298.
[31] R. Horn, K.A. Williams, N.J. Degenstein, A. Bitsch-Larsen, D. Dalle Nogare, S.A. Tupy, L.D. Schmidt, J. Catal. 249 (2007) 380.
[32] A. Beretta, T. Bruno, G. Groppi, I. Tavazzi, P. Forzatti, Appl. Catal. B 70 (2007) 515.
[33] S. Hannemann, J.-D. Grunwaldt, N. van Vegten, A. Baiker, P. Boye, C.G. Schroer, Catal. Today 126 (2007) 54.
[34] J.R. Rostrup-Nielsen, J. Catal. 31 (1973) 173.
[35] Y. Wang, Y. Chin, R. Rozmiarek, B. Johnson, Y. Gao, J. Watson, A. Tonkovich, D. Vander Wiel, Catal. Today 98 (2004) 575.
[36] P. Dauenhauer, J. Salge, L. Schmidt, J. Catal. 244 (2006) 238.
[37] J. Rostrup-Nielsen, J.-H. Bak Hansen, J. Catal. 144 (1993) 38.
[38] J.B. Claridge, H.L.H. Green, S.C. Tsang, Catal. Today 21 (1994) 455.
[39] P. Aparicio, A. Guerrero-Ruiz, I. Rodrguez-Ramos, Appl. Catal. A 170 (1998) 177.
[40] P. Ferreira-Aparicio, M. Fernandez-Garcia, A. Guerrero-Ruiz, I. Rodrgues-Ramos, J. Catal. 190 (2000) 296.
[41] J.F. Múnera, S. Irusta, L.M. Cornaglia, E.A. Lombardo, D.V. Cesar, M. Schmal, J. Catal. 245 (2007) 25.
[42] S. Ayabe, H. Omoto, T. Utaka, R. Kikuchi, K. Sasaki, Y. Teraoka, K. Eguchi, Appl. Catal. A 241 (2003) 261.
[43] B. Li, K. Maruyama, M. Nurunnabi, K. Kunimori, K. Tomishige, Appl. Catal. A 275 (2004) 157.
[44] B. Dreyer, I. Lee, J. Krummenacher, L. Schmidt, Appl. Catal. A 307 (2006) 184.
[45] W.Z. Weng, M.S. Chen, Q.G. Yan, T.H. Wu, Z.S. Chao, Y.Y. Liao, H.L. Wan, Catal. Today 63 (2000) 317.
[46] Q. Zhu, X. Zhao, Y. Deng, J. Nat. Gas. Chem. 13 (2004) 191.
[47] K. Walter, O. Buyevskaya, D. Wolf, M. Baerns, Catal. Lett. 29 (1994) 261.
[48] O. Buyevskaya, K. Walter, D. Wolf, M. Baerns, Catal. Lett. 38 (1996) 81.
[49] O. Buyevskaya, D. Wolf, M. Baerns, Catal. Lett. 29 (1994) 249.
[50] I. Aartun, B. Silberova, H. Venvik, P. Pfeifer, O. Görke, K. Schubert, A. Holmen, Catal. Today 105 (2005) 469.

[51] K. Schubert, W. Bier, J. Brandner, M. Fichtner, C. Franz, G. Linder, Proceedings of the Second International Conference on Microreaction Technology (IMRET 2), 8–12 March, New Orleans, 1998.
[52] B. Silberova, H.J. Venvik, A. Holmen, Catal. Today 99 (2005) 69.
[53] A. Kölbl, P. Pfeifer, M. Kraut, K. Schubert, M. Fichtner, M. Liauw, G. Emig, Chem. Eng. Technol. 27 (2004) 671.
[54] H. Phillips, Combust. Flame 7 (1963) 129.
[55] M.T. Janicke, H. Kestenbaum, U. Hagendorf, F. Schth, M. Fichtner, K. Schubert, J. Catal. 191 (2000) 282.
[56] P. Pfeifer, L. Bohn, O. Görke, K. Haas-Santo, U. Schygulla, K. Schubert, Chem. Eng. Technol. 28 (2005) 439.
[57] B. Silberova, H. Venvik, J. Walmsley, A. Holmen, Catal. Today 100 (2005) 457.
[58] H.-Y. Lin, Y.-W. Chen, C. Li, Thermochim. Acta 400 (2003) 61.
[59] D.L. Hoang, H. Lieske, Thermochim. Acta 345 (2000) 93.
[60] A. Stefanescu, A.C. van Veen, C. Mirodatos, J.C. Beziat, E. Duval-Brunel, Catal. Today 125 (2007) 16.
[61] F. Basile, G. Fornasari, F. Trifirò, A. Vaccari, Catal. Today 77 (2002) 215.
[62] S. Irusta, L.M. Cornaglia, E.A. Lombardo, J. Catal. 210 (2002) 7.
[63] S. Irusta, L.M. Cornaglia, E.A. Lombardo, J. Catal. 210 (2002) 263.
[64] W.K. Jóźwiak, M. Nowosielska, J. Rynkowski, Appl. Catal. A 280 (2005) 233.
[65] D. Hickman, E. Haupfear, L. Schmidt, Catal. Lett. 17 (1993) 223.
[66] K. Heitnes, S. Lindberg, O. Rokstad, A. Holmen, Catal. Today 21 (1994) 471.
[67] M.J. Hei, H.B. Chen, J. Yi, Y.J. Lin, G. Wei, D.W. Liao, Surf. Sci. 417 (1998) 82.
[68] M.G. Cutrufello, S. De Rossi, I. Ferino, R. Monaci, E. Rombi, V. Solinas, Thermochim. Acta 434 (2005) 62.
[69] B.N.T. Nguyen, C.A. Leclerc, J. Power Sources 163 (2007) 623.
[70] D.R. Lide (Ed.), CRC Handbook of Chemistry and Physics, CRC Press, 2005.
[71] L. Basini, A. Guarinoni, A. Aragno, J. Catal. 190 (2000) 284.
[72] B. Li, S. Kado, Y. Mukainakano, M. Nurunnabi, T. Miyao, S. Naito, K. Kunimori, K. Tomishige, Appl. Catal. A 304 (2006) 62.
[73] B. Li, R. Watanabe, K. Maruyama, K. Kunimori, K. Tomishige, Catal. Today 104 (2005) 7.
[74] F. Cavani, F. Trifiró, Catal. Today 24 (1995) 307.
[75] M. Huff, L.D. Schmidt, J. Catal. 149 (1994) 127.
[76] A. Beretta, P. Forzatti, E. Ranzi, J. Catal. 184 (2007) 469.
[77] M. Xu, J.H. Lunsford, React. Kinet. Catal. Lett. 57 (1996) 3.
[78] J.B. Claridge, M.L. Green, S.C. Tsang, A.P. York, A.T. Ashcroft, P.D. Battle, Catal. Lett. 22 (1993) 299.
[79] Y. Ji, W. Li, H. Xu, Y. Chen, React. Kinet. Catal. Lett. 73 (2001) 27.
[80] A. Holmen, O. Olsvik, O.A. Rokstad, Fuel Process. Technol. 42 (1995) 249.